

Article

Stiffness Analysis and Verification of Hydraulic Supporting Units for In-Situ Optical Testing of a 500 mm-Diameter Mirror

Deyi Dong ¹, Di Zhou ^{1,*}, Yuhan Jiang ², Lianqiang Wang ¹, Chao Li ¹, Haifei Hu ¹, Yingjun Guan ³ and Minghui Gao ¹

¹ Changchun Institute of Optics, Fine Mechanics and Physics, Chinese Academy of Sciences, Changchun 130033, China

² Canon Medical System Research Development (Dalian) Co., Ltd., Dalian 116085, China

³ College of Mechanical & Electrical Engineering, Changchun University of Technology, Changchun 130012, China

* Correspondence: zhoudi@ciomp.ac.cn

Abstract: A hydraulic in-situ support system is commonly used in the optical testing of mirrors, since it is convenient to unload the gravity of a mirror to be measured without the risk of being turned over or moved to another place. The existing supporting structures have several disadvantages, such as the problem of the output force deviating from the axis, being sensitive to machining loads, its flexible components easily leading to fatigue damage by cyclic loads and so on. A new single-cylinder hydraulic supporting unit with a ball hinge was proposed, analyzed and verified in this paper. A finite simulation based on four structural parameters' effect on the stiffness of the proposed hydraulic supporting unit showed that increasing the thickness, elastic modulus and convolution width of the rolling diaphragm and decreasing the height of the rolling diaphragm to some extent was beneficial to a high stiffness. Moreover, it could be concluded from experiments that, in order to decrease the stiffness dispersion, the air ratio should be as low as possible and the values of the initial pressure and press speed should be as high as possible. These results are conducive to maintain a high stiffness of HSU to bear the processing load and reduce the low-order aberrations of mirror which provide a reference for future hydraulic supporting unit designs.

Keywords: in-situ optical testing; hydraulic supporting unit; axial stiffness; stiffness dispersion



Citation: Dong, D.; Zhou, D.; Jiang, Y.; Wang, L.; Li, C.; Hu, H.; Guan, Y.; Gao, M. Stiffness Analysis and Verification of Hydraulic Supporting Units for In-Situ Optical Testing of a 500 mm-Diameter Mirror. *Machines* **2022**, *10*, 828. <https://doi.org/10.3390/machines10100828>

Academic Editor: Feng Gao

Received: 1 August 2022

Accepted: 14 September 2022

Published: 21 September 2022

Publisher's Note: MDPI stays neutral with regard to jurisdictional claims in published maps and institutional affiliations.



Copyright: © 2022 by the authors. Licensee MDPI, Basel, Switzerland. This article is an open access article distributed under the terms and conditions of the Creative Commons Attribution (CC BY) license (<https://creativecommons.org/licenses/by/4.0/>).

1. Introduction

The surface shape of a reflector manufactured under ground gravity constraints will change after the camera enters orbit, due to the release of gravity [1–5]. The traditional ways of manufacturing and testing optical mirrors are implemented separately, which cause great risks, especially when the workpiece is turned over or moved to another place for testing [6–8]. Compared to traditional testing methods, the in-situ optical testing of mirrors has many advantages, such as saving much time, workload and budget [9]. Furthermore, the hydraulic in-situ support system turns out to be an effective way of realizing in-situ optical testing, owing to its advantages such as a fast response, high axial stiffness and reducing the print through effect of polishing mirrors [10]. The hydraulic in-situ support system is usually composed of several hydraulic supporting units and some accessories. The mirror support structure should achieve two basic functions: one is to determine the position of the mirror space, and the other is to maintain the accuracy of the mirror shape [11,12]. In order to ensure a high surface figure and reduce low-order surface shape errors such as the dispersion, coma and trefoil dispersion of supported mirror surfaces for testing, either we increase the axial stiffness of a hydraulic supporting unit (short for HSU) [13,14] or reduce the stiffness dispersion of several HSUs [15]. Pneumatic and hydraulic supporting units are the two main supporting units utilized in some mainstreaming hydraulic systems. Pneumatic supporting units, like the supporting unit used for the

6.5 m aperture main mirror of the Multi-Mirror Telescope (MMT), are composed of a dual pneumatic cylinder, a buffer and a force actuator [16]. However, gases are more easily compressed, resulting in lower support stiffness. Therefore, the pneumatic support unit is more sensitive to the processing load, which is not conducive to obtaining high-surface-shape accuracy. Hydraulic supporting units are mainly divided into two kinds of structures, including dual-cylinder supporting units [17,18] and single-cylinder supporting units [19]. As for the dual-cylinder supporting units, the support force is output by means of the differential hydraulic pressures of the upper and lower chambers. On the one hand, the dual-cylinder structure is complicated, which is difficult to be processed and assembled with increasing the processing budget. On the other hand, more components of HSU will bring more risks of fluid leakage. A typical structure of the single-cylinder supporting units is the HSU used for the SUBARU 8.3 m main mirror, which consists of a buffer and a single hydraulic cylinder. However, this structure possesses the problem of the uneven distribution of floating masses and the deviation of output forces from the axis caused by the side exhaust scheme. Moreover, the buffer and force feedback element attached to the top of the support structure make it difficult to integrate and control the support system, and the cost of manufacturing the support unit is even more expensive. Therefore, the structure of HSU needs to be simplified furthermore and needs to keep a good working performance. Furthermore, considering that the cyclic loads from the grinding head can easily lead to fatigue damage to flexible components of HSU, it is essential to design a simplified single-cylinder supporting unit to overcome the above problems. In this paper, a single-cylinder hydraulic support structure with a ball joint is proposed. Since the stiffness of the HSU is directly relevant to whether the HSU is sensitive to the processing load or not, the factors influencing a HSU's stiffness are investigated analytically and experimentally. The dispersion of several HSUs' stiffness needs to be reduced to acquire a high surface figure of the mirror.

2. Illustration of HSU Design and Working Principle

A pneumatic hydraulic composite support system, as shown in Figure 1, is utilized to simulate the state of a mirror's surface figure under processing or testing. When the mirror is under processing, nine HSUs will bear the gravity of the mirror and the grinding load. After the manufacture of the mirror, nine HSUs will descend to a lower altitude, and the rolling diaphragm will rise to bear the gravity of the mirror for testing. In this paper, we only focus on the state of the mirror being under processing. Nine HSUs are fixed on the foundation, and when these HSUs are working, the spherical mirror will rise a certain height.

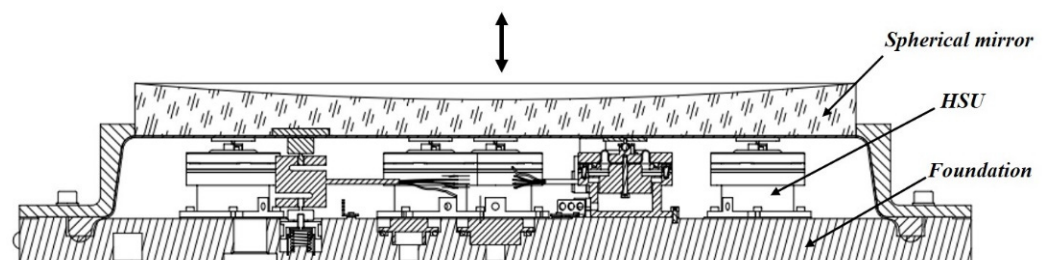


Figure 1. Schematic of a profile of a pneumatic–hydraulic composite support system.

As depicted in Figure 2, nine HSUs are distributed uniformly in the circular direction. Each HSU in the inner circle and every two HSUs in the outer circle share one peristaltic pump. Each HSU in this combination possesses the same pressure of the working liquid.

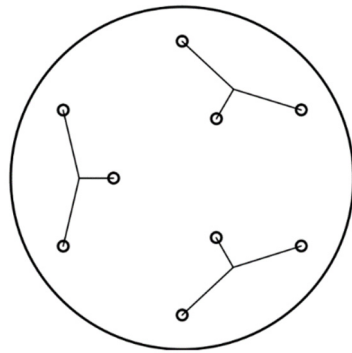


Figure 2. Schematic diagram of the connection of support units.

The single-cylinder HSU with a ball hinge is presented in Figure 3. The support unit, from top to bottom, consists of a ball hinge, an upper flange, a lower flange, a rolling diaphragm, a gasket, a piston and a cylinder block. All components of the supporting unit are made of aluminum alloy (i.e., 2A12) except the gasket and rolling diaphragm whose material are NBR. The sealing connector can be easily purchased since it is a standard component. The design focuses on three points: 1. ensuring the sealing of the HSU; 2. maintaining the rolling performance of the moving parts; 3. reducing the damage of the grinding head to the flexible parts in the support unit. Among them, the sealing performance is mainly guaranteed by a combination of the ring rubber strip of the rolling diaphragm, the groove of the flange end cover, the rubber gasket and the sealing connector. The rolling performance of the moving parts is mainly achieved by selecting an appropriate rubber material for the rolling diaphragm and manually convolving the rolling part of the diaphragm. Moreover, reducing the damage of the flexible part is achieved by the universal ball hinge at the top of the HSU.

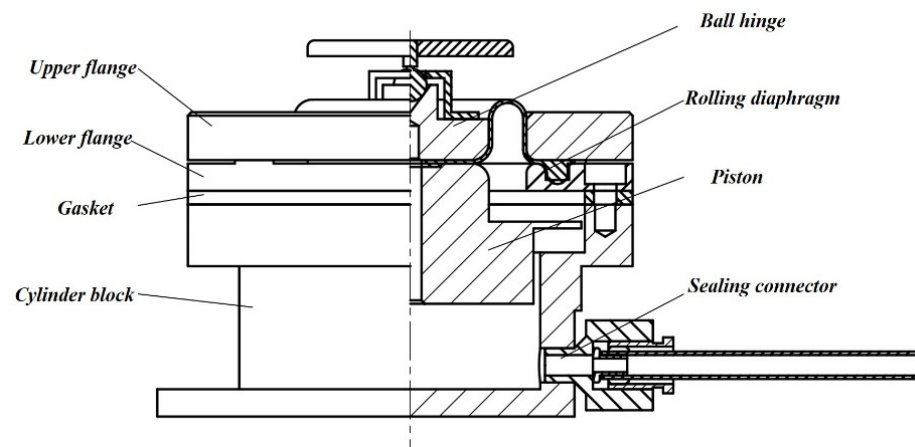


Figure 3. Half-sectional diagram of the proposed single-cylinder HSU.

The working principle of HSU is described as follows. A cylinder block, piston, rolling diaphragm, upper flange, lower flange and gasket constitute a closed vacuum chamber. The side of the cylinder block is equipped with an oil port and is connected to the hydraulic line. When the vacuum chamber is oiled, the rolling diaphragm bears the tensile load inside the cylinder block and rolls along the axis, pushing the floating component up. After the mirror's back comes into contact with the HSU, the unloading of the mirror's gravity begins. The HSU has the characteristics of negligible lateral stiffness and large axial stiffness. The ball joint at the top can be rotated freely, achieving a better fit with the mirror back. It is conducive to the decoupling of multi-axis stiffness when used for unloading the gravity of the mirror.

3. Theoretical Consideration of the Stiffness of a HSU

After the oil inlet of a HSU is opened and filled with liquid, the mirror is raised to a certain height and reaches a steady state. As shown in Figure 4, considering that a HSU is hydrostatically balanced, the pressure of liquid is defined as P ; the mass of the ball hinge, m_1 ; the mass of the piston, m_2 ; the gravity of the floating component, G ; the tension of the rolling diaphragm, Ft ; the force of the mirror on the HSU, F_0 ; the sum of the internal pressure of the HSU, F . Then the force balance equation of the HSU is:

$$F = G + F_0 + Ft \quad (1)$$

wherein, the working radius of the rolling diaphragm is R ; the convolution width of the diaphragm, C ; the thickness of the rolling diaphragm, t . Since the convolution width C is relatively larger than the thickness t , it is assumed that the cross-section tensile stress caused by the diaphragm tension Ft is evenly distributed along the thickness t direction. According to the reference [10], the total pressure acting in a certain direction on the surface is equal to the product of the projection area and the pressure of the compression surface in this direction. Thus the diaphragm tension Ft , the gravity G of the floating component and the sum of the internal pressure of HSU F are:

$$Ft = \pi(2RC - C^2)P \quad (2)$$

$$G = (m_1 + m_2)g \quad (3)$$

$$F = \pi R^2 P \quad (4)$$

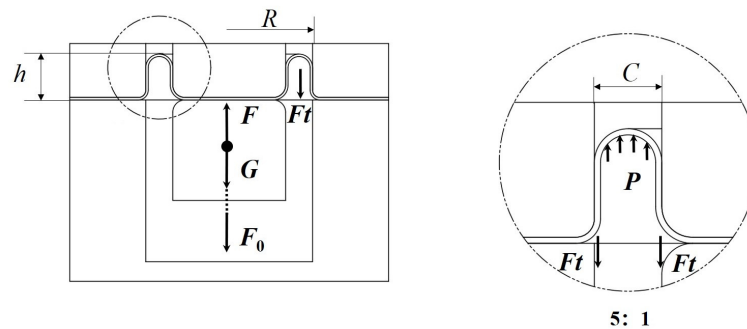


Figure 4. Schematic diagram of axial force analysis of the HSU.

According to Equations (1)–(4), it can be deduced that the force F_0 of the mirror on HSU is:

$$F_0 = \pi(R - C)^2 P - (m_1 + m_2)g \quad (5)$$

The axial stiffness S of HSU is defined as the ratio of the unit output force to the axial displacement per unit of cylinder head, that is:

$$S = \frac{dF_0}{ds} \quad (6)$$

When the structural parameters of HSU are determined, the unit output force is derived from Equation (5):

$$dF_0 = \pi(R - C)^2 dP = -\pi(R - C)^2 K \frac{dV}{V} \quad (7)$$

where K is the volume modulus of the liquid, and V is the working volume of HSU. Since the rolling diaphragm material is NBR rubber, which has a certain elasticity, it will be stretched for a certain length during the lifting of the mirror. The total length of the

stretchable part of the diaphragm is l , and the diaphragm stretch is dl , then the liquid working volume change of HSU dV is shown in Formula (8).

$$dV = \pi(R - C)^2 ds - \pi RC \left(\frac{ds + dl}{2} \right) \quad (8)$$

According to the mechanics of the material, the elongation of the diaphragm dl is equal to:

$$dl = \frac{Cl}{2Et} dp \quad (9)$$

where E is the modulus of elasticity of the diaphragm, and t is the thickness of the diaphragm.

According to Formulas (6)–(9), the axial stiffness S of HSU can be derived as:

$$S = \frac{\pi^2(R - C)^2(R - 2C)(2R - C)}{\pi RC^2 l / 2Et - 2V/K} \quad (10)$$

From Equation (10), it can be seen that the axial stiffness of HSU is related to the structural parameters, including the working radius of the rolling diaphragm R , the convolution width the diaphragm C , the thickness of the diaphragm t , the elastic modulus of the diaphragm material E , the working volume of the liquid filled V , and the volume modulus K .

4. Stiffness Simulation Analysis of HSU

In this section, a static analysis under typical working conditions is performed to further investigate the key parameters affecting the stiffness of the HSU, which also verifies the deduction of theory.

Given that the sum of the supporting forces of three HSUs in the inner circle and the sum of the supporting forces of six HSUs in the outer circle is equal to the gravity of the mirror, the RMS minimum value of the mirror surface type is set as the objective function. Through optimization iteration, the optimal result is that, when the support force of the three support points in the inner circle is 15.63 N and the support force of the six support points in the outer circle is 17.02 N, the surface RMS value of the mirror is the smallest. In order to simulate the gravitational deformation of the mirror in actual working conditions, a cylinder with a small elastic modulus is set in the center of the mirror back to impose a fixed constraint. Parameters set in the finite simulation is shown in Table 1. The specific finite element model is shown in Figure 5a.

The mirror body is endowed with the corresponding material parameters of glass-ceramic. The PV value of the nine-point support of the mirror in the ideal state is 46.7 nm, and the RMS value is 9.4 nm. The deformation of the mirror body is shown in Figure 5b.

Table 1. Simulation conditions set in Hypermesh.

	Parameters	Values
NBR	Young modulus	3.5 MPa
	Density	9.8×10^{-10} t/mm ³
	Poisson's ratio	0.45
2A12	Young modulus	68,000 MPa
	Density	2.8×10^{-10} t/mm ³
	Poisson's ratio	0.25
glass-ceramic	Young modulus	90,600 MPa
	Density	2.53×10^{-9} t/mm ³
	Poisson's ratio	0.24

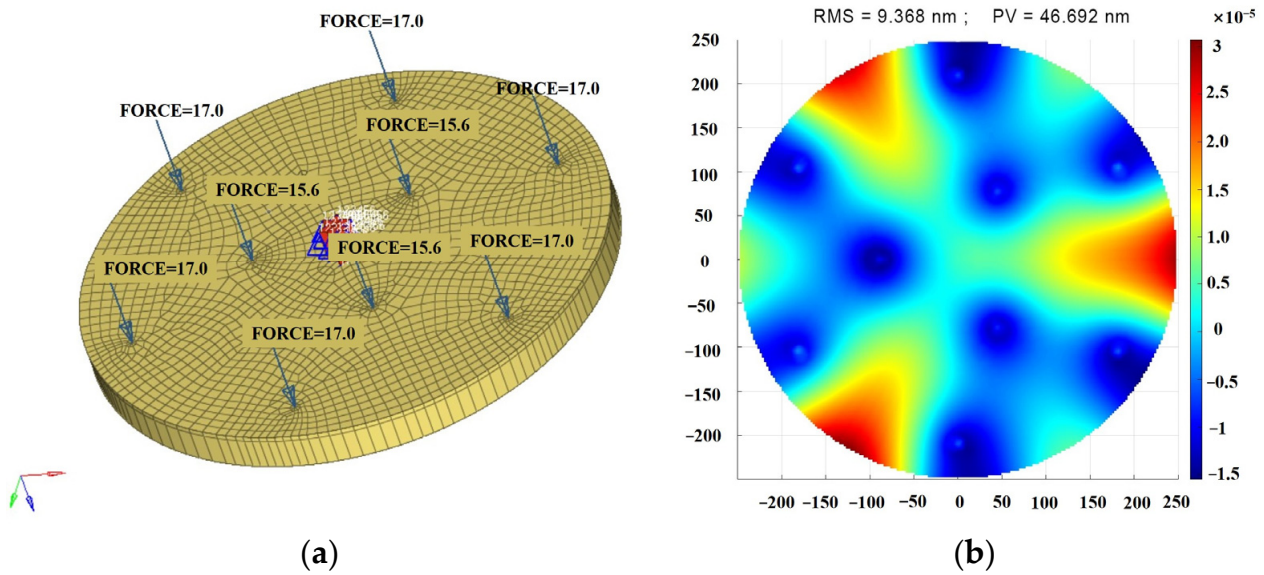


Figure 5. (a) Finite element model of the 500 mm diameter mirror; (b) finite result of the 500 mm mirror’s deformation.

Based on typical working conditions, the support pad of the HSU is subjected to a vertical downward pressure of 17 N, and the internal pressure of the hydraulic chamber is 42.3 kPa. The bottom of the HSU’s finite model is fixed. In order to reduce the amount of calculation, the spherical joints, oil ports and other parts that have little influence on the structural force are omitted from the model.

The cloud diagram of the calculation results is shown in Figure 6. Figure 6a is the overall deformation cloud diagram of the HSU under typical working conditions, and Figure 6b is the deformation cloud diagram of the floating parts in HSU under the corresponding working conditions. It can be seen from the figure that the axial displacement of the floating part is 0.641 mm, and the displacement in the radial direction is almost negligible, which clearly shows that the HSU has no lateral stiffness. Therefore, this kind of structure is suitable for the gravity unloading of large-diameter mirrors.

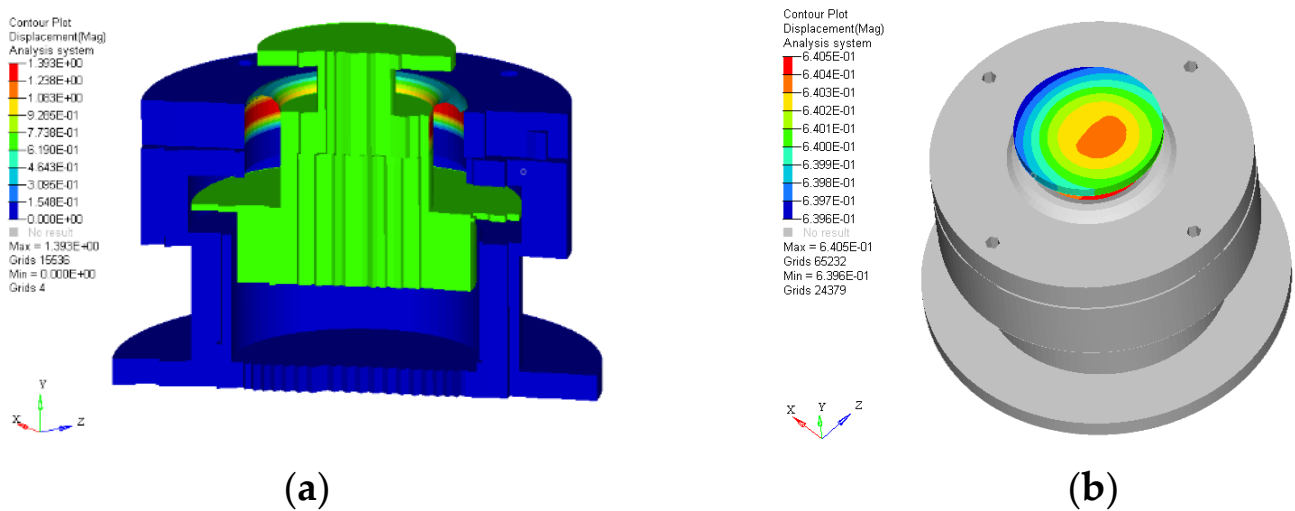


Figure 6. (a) Overall deformation cloud diagram of HSU; (b) deformation cloud diagram of the floating parts.

In this section, the effects of rolling film thickness t , convolution width C , film height h and elastic modulus E on support stiffness are determined by finite element analysis.

Using 10 sets of data within the range of $\pm 20\%$ of original structural parameters and $\pm 14\%$ of the elastic modulus of the rolling diaphragm for finite element analysis, the design values and variation ranges of the various parameters are shown in Table 2.

Table 2. Values of structural parameters in simulation analysis.

	Initial Value	Minimum	Maximum
t (mm)	0.5	0.4	0.6
C (mm)	5.5	4.4	6.6
h (mm)	8.8	7	10.6
E (MPa)	3.5	3.0	4.0

To ensure the accuracy of the results, a single variable should be controlled, and other parameters should remain unchanged during the finite element analysis.

The influence curves of stiffness versus values of different parameters are shown in Figure 7a–d. It can be seen that, basically, the simulation results are consistent with the theoretical deduction. As the diaphragm thickness grows, the stiffness of the HSU keeps rising, as is the elastic modulus of the rolling diaphragm. The difference between the two curves is that the growth rate of the former one keeps increasing, while that of the latter one descends. The height and width of the convolution part also influence the stiffness of the HSU to some extent. Comparing Figure 7a,b, the trend of these two curves is almost opposite. Moreover, even though the stiffness of the HSU increases as the width of the convolution part increases, the curve is rising with some jitters since the working volume V is influenced by the width of the convolution part, which is consistent with the theoretical results.

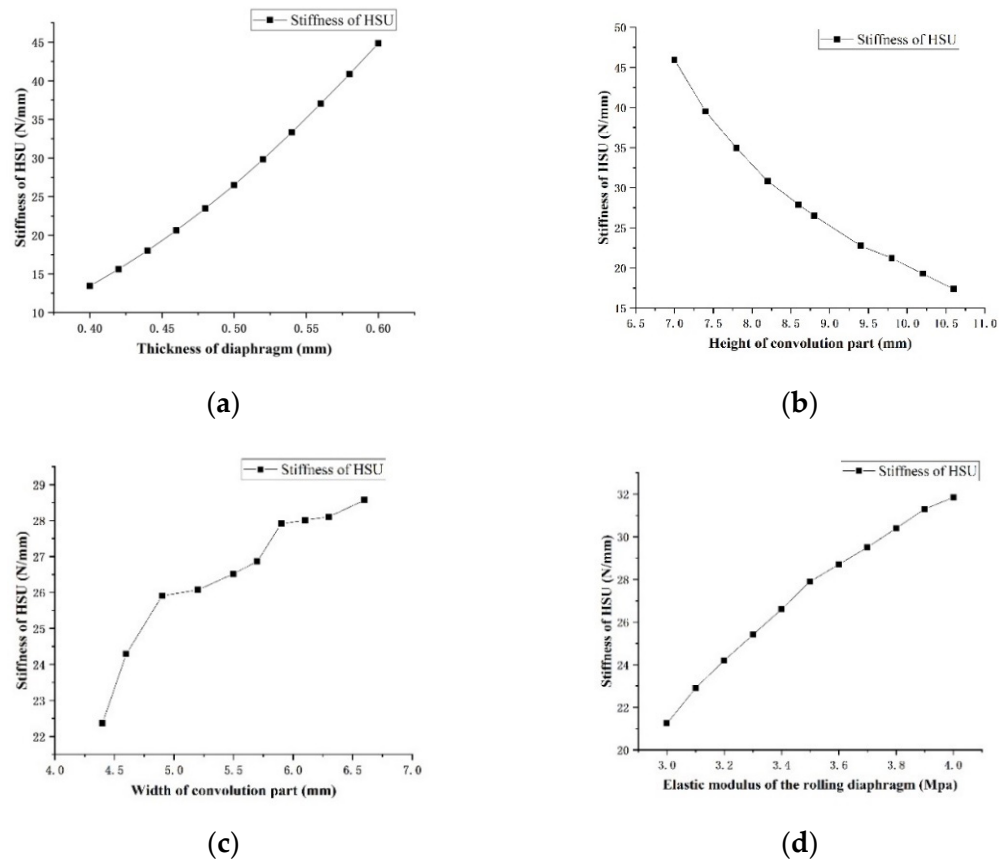


Figure 7. (a) Effect of the rolling diaphragm thickness on support stiffness; (b) effect of the rolling diaphragm convolution height on support stiffness; (c) effect of the rolling diaphragm convolution width on support stiffness; (d) effect of elastic modulus on support stiffness.

5. Experimental Verification

In order to reduce the stiffness dispersion, it is necessary to strictly follow the tolerance when processing the diaphragm and to control the error within a certain range, which helps to reduce the difference in support stiffness, so as to obtain better gravity unloading accuracy. Four structural parameters are all investigated by finite element analysis in an ideal state to determine the key factors affecting the stiffness of the support, but there are still some other factors in actual states, such as bubble content, initial pressure and pressing speed, which also influence the stiffness of the HSU. Therefore in this section, a testing platform is built so as to further explore factors in the stiffness and stiffness dispersion.

The instrument required for the test is an electronic universal testing machine (DDL10). It is cascaded with a force sensor with a range of 200 N. The effective measurement range of force is 0.4–100% FS. The testing machine is equipped with a high-precision displacement sensor and TestExpert.NET software V1.0 (Sinotest Equipment Co., Ltd., Changchun, China), which can record the deformation of the workpiece while adjusting the force. The force measurement accuracy and deformation measurement accuracy are $\pm 0.5\%$ of the indicated value. The testing diagram of the HSU on the testing machine is shown in Figure 8. The values of some key structural parameters of the HSU are summarized as follows. The axial adjustment distance of the HSU is 8 mm; the working diameter, 65 mm; the axial height, 55 mm; the working radius of the rolling diaphragm R , 17 mm; the convolution width C , 5.5 mm; the thickness of the rolling diaphragm t , 1 mm; the radius of the dome hinge top cover, 14 mm.



Figure 8. HSU on the testing machine.

A specific connection method is shown in Figure 9. A peristaltic pump (BT103S) possesses the ability of adjust the speed and stabilize the pressure. It is equipped with a Y25 pump head. The piezometer (SN-C530) with a range of 0 to 100 kPa is to monitor the pressure of the HSU, considering that the stiffness of the HSU is relevant to the initial pressure of the working liquid. The piezometer uses the RS-485 protocol to communicate with a PC and shows the pressure of the liquid in real time. When the pipe pressure reaches the setting value, the ball valve is shut down to maintain the pressure. Additionally, the self-made connector is to connect two hoses of different sizes. To be noted, the working liquid used in this experiment is water. Special attention should be paid during the connection process: the test requires good sealing, so the connection of each element of the circuit should be completely sealed, and each interface can be sealed with raw tape.

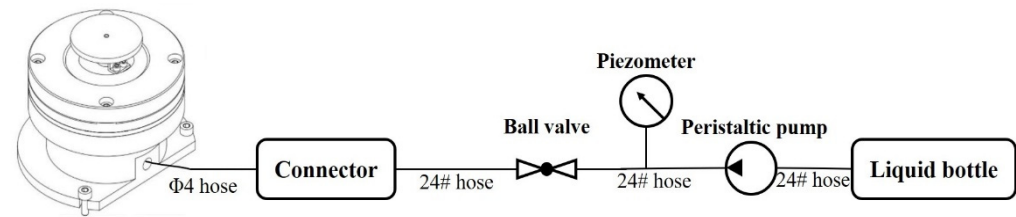


Figure 9. Diagram of the stiffness testing system.

Without any processing stress, according to Equations (1)–(5), the original pressure of the working liquid can be calculated (i.e. 42.3 kPa) when the HSU reaches a steady state. The maximum load was set as 20 N, and the slope of the deformation value of the HSU and difference between a load of 16 N and of 18 N is calculated. The simulated result of the HSU's stiffness with a load of 17 N is about 26.521 N/mm. And the experimental result is about 26.16 N/mm. The difference between the simulated result and the experiment is less than 1.4%.

Referring to [20], for this single-cylinder supporting unit with only axial stiffness, the stiffness of the HSU descends as the air bubble content increases. Considering the complexity of simulation analysis involving air, fluid and solid, it is more convenient to verify the influence of air bubble content on the stiffness of the HSU qualitatively by experiments. Before the HSU is filled with the working liquid, the remaining air in the HSU will be extracted by the peristaltic pump as much as possible. Then the switch of the peristaltic pump is reversed, and the HSU is filled with air for three seconds as a unit before the HSU is supplied with the working liquid. Given that the speed of the peristaltic pump is constant once set, the air ratio is positively correlated with the working time of filling air into the HSU. According to the product brochure of the peristaltic pump with a Y25 pump head and 24# tube, once the revolutions per minute (rpm) of the pump is set to 100, the flow rate is about 283 mL/min. Thus the total volume of air pumped into the HSU in three seconds can be calculated as 14.15 mL. The working volume of the HSU is about 27,107 mL. Therefore one unit of air ratio is about 0.05%. The result of the effect of the air ratio on the stiffness of the HSU is shown in Figure 10. The relation is nearly inversely proportional. It is mainly because gas is compressed more easily than liquid. Therefore, before the HSU is put into use, the air bubble in the pipeline and the HSU should be removed as much as possible.

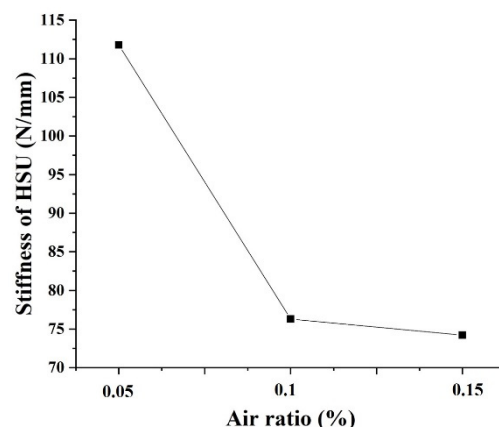


Figure 10. Curve of the stiffness of the HSU versus the air ratio.

In order to study the effect of different pressures in the oil pipeline on the dispersion of the support stiffness, the stiffness of the three HSUs in the above-mentioned combination was measured. The content of air bubbles and the pressure of the pipeline are adjusted by the peristaltic pump. The stiffness value of each HSU was measured at 50 kPa, 70 kPa, 100 kPa and 120 kPa, respectively, and the average value of the support stiffness and the

average value of the offset were calculated, and the average value of the offset of each group with different pressure values was compared. As depicted in Figure 11, the greater the pressure, the lower the stiffness dispersion, and when the pressure increases, the support stiffness increases significantly. Therefore, a high liquid pressure should be maintained within the safe working range of the entire system.

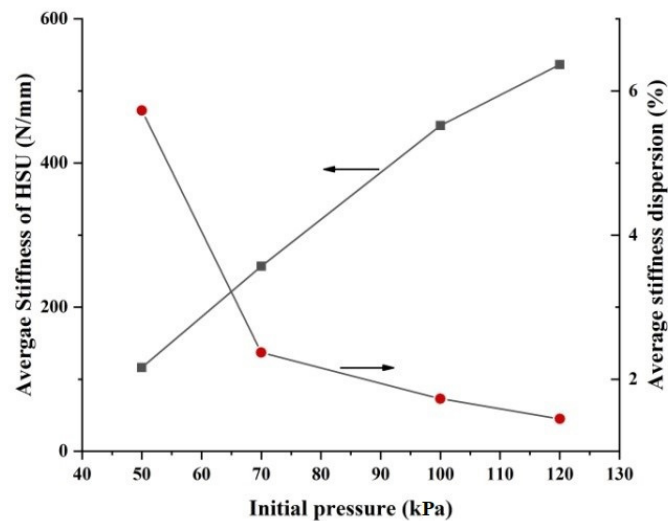


Figure 11. Average stiffness and stiffness dispersion of HSUs versus various initial pressure values.

For 3 HSUs for stiffness tests under 100 kPa, each HSU can be measured under indenter pressing speeds of 0.1 mm/min, 0.2 mm/min, 0.3 mm/min, 0.4 mm/min and 0.5 mm/min, respectively. The mean value of the support stiffness and the mean value of the deviation were calculated. The results of each of the HSUs in five groups are compared. It can be concluded that the smaller the mean value, the lower the stiffness dispersion. From Figure 12, it can be seen that the workpiece pressing speed has a significant effect on the stiffness dispersion. The faster the pressing speed is, the smaller the deviation, and the lower the stiffness dispersion.

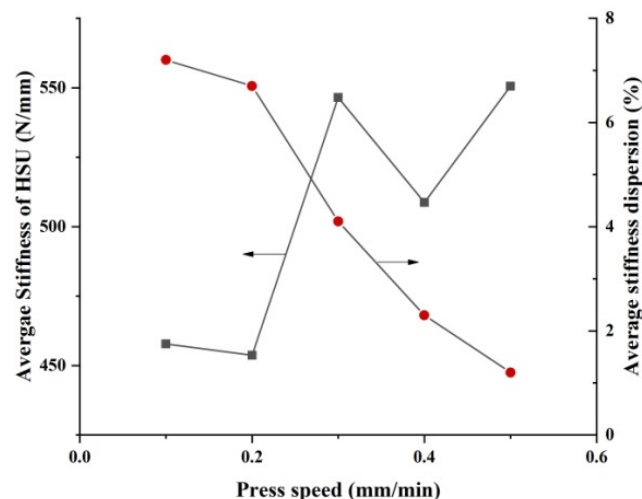


Figure 12. Average stiffness and stiffness dispersion of HSUs versus various press speeds.

6. Conclusions

In this paper, a new single-cylinder HSU is proposed, analyzed by theory and simulation and verified with several experiments. Compared with existing hydraulic support units, the proposed HSU in this paper has the following advantages: 1. The design follows the principle of rotational symmetry to ensure that the output support force is along the

axis; 2. The new hydraulic support unit using a liquid medium can provide greater stiffness, which can reduce the self-weight deformation of the mirror body and can be less sensitive to the processing load, so as to achieve the inhibition of the imprinting effect; 3. The universal spherical hinge structure is adopted, which solves the problem that the circulating load easily leads to fatigue damage to flexible components; 4. The buffer structure and force feedback element attached to the top of the support structure are removed, making the support system integration and control easier and the manufacturing cost lower. A finite simulation based on four structural parameters' effect on the stiffness of the HSU shows that increasing the thickness, elastic modulus and convolution width of the rolling diaphragm and decreasing the height of the rolling diaphragm to some extent is beneficial to a high stiffness of the HSU. Moreover, it can be concluded from experiments that, in order to decrease the stiffness dispersion, the air ratio should be as low as possible and the values of the initial pressure and press speed should be as high as possible. Considerably more work will need to be done to perfect the proposed structure of a single-cylinder HSU, such as adding an exhaust-recirculation structure with a plug in order to expel the remaining air from the HSU to keep a high axial stiffness. Additionally, since the liquid inside the hydraulic cylinder is compressible, the effect of the hydraulic medium on the support stiffness should also be investigated carefully.

Author Contributions: Writing—review and editing, D.D.; writing—original draft preparation, D.Z.; validation, Y.J., L.W. and H.H.; supervision, C.L.; project administration, M.G.; funding acquisition, Y.G. All authors have read and agreed to the published version of the manuscript.

Funding: This research was funded by National Natural Science Foundation of China, grant number 11873007 and 62175234.

Institutional Review Board Statement: Not applicable.

Informed Consent Statement: Not applicable.

Data Availability Statement: Not applicable.

Acknowledgments: This research work was supported by National Natural Science Foundation of China, grant number 11873007 and 62175234.

Conflicts of Interest: The authors declare no conflict of interest.

References

1. Pradeep, K.K.V.; Maruthi, B.H.; Krishnamurthy, T. Design and analysis of three axis gimbal mount for testing a large size light weight mirror of a space borne telescopic optics. *Int. J. Res. Aeronaut. Mech. Eng.* **2013**, *1*, 16–36.
2. Martin, H.M.; Allen, R.G.; Burge, J.H.; Dettmann, L.R.; Ketelsen, D.A.; Miller, S.M., III; Sasian, J.M. Fabrication of mirrors for the Magellan telescopes and the Large Binocular Telescope. *Proc. SPIE* **2003**, *4837*, 609–618.
3. Bittner, H.; Erdmann, M.; Herdt, B.; Steinacher, A. The Optical System of the SOFIA Telescope. *Proc. SPIE* **2004**, *5489*, 805–816.
4. Lampton, M.L.; Akerlof, C.W.; Aldering, G.; Amanullah, R.; Astier, P.; Barrelet, E.; Bebek, C.; Bergstrom, L.; Bercovitz, J.; Bernstein, G.; et al. SNAP Telescope. *Proc. SPIE* **2002**, *4849*, 215–226.
5. Toulemont, Y.; Breyse, J.; Pierot, D.; Sein, E.; Nakagawa, T.; Kaneda, H.; Onaka, T.; Hirabayashi, M.; Narasaki, K.; Sakuta, H.; et al. The 3.5m all SiC Telescope for SPICA. *Proc. SPIE* **2004**, *5487*, 1001–1012.
6. Bloemhof, E.E.; Lam, J.C.; Fera, V.A.; Chang, Z. Extracting the zero-gravity surface figure of a mirror through multiple clockings in a flightlike hexapod mount. *Appl. Opt.* **2009**, *48*, 4239–4245. [[CrossRef](#)] [[PubMed](#)]
7. Hu, H.; Qi, E.; Luo, X.; Zhang, X.; Xue, D. Rapid fabrication strategy for $\phi 1.5$ m off-axis parabolic parts using computer-controlled optical surfacing. *Appl. Opt.* **2018**, *57*, F37–F43. [[CrossRef](#)] [[PubMed](#)]
8. Bloemhof, E.E.; Lam, J.C.; Fera, V.A.; Chang, Z. Extracting the zero-gravity surface figure of a mirror. In Proceedings of the Optical and Infrared Interferometry, Marseille, France, 28 July 2008; pp. 1177–1188.
9. Yu, G.; Walker, D.D.; Li, H. Research on fabrication of mirror segments for E-ELT. In Proceedings of the 6th International Symposium on Advanced Optical Manufacturing and Testing Technologies (AOMATT 2012), Xiamen, China, 16 October 2012; pp. 19–24.
10. Hu, H.; Luo, X. Design scheme for optical manufacturing support system of TMT M3 prototype. In Proceedings of the 7th International Symposium on Advanced Optical Manufacturing and Testing Technologies: Large Mirrors and Telescopes, Harbin, China, 2 September 2014; pp. 28–33.
11. Yoder, P.R. *Mounting Optics in Optical Instruments*; SPIE Press: Bellingham, WA, USA, 2008; p. 579.

12. Wells, C.; Whitman, T.; Hannon, J.; Jensen, A. Assembly integration and ambient testing of the James Webb Space Telescope primary mirror. *Proc. SPIE* **2004**, *5487*, 859–866.
13. L, J.F. Research on the Design of Cylinder Used as the Primary Mirror Support of Telescope. *J. Chang. Univ. Sci. Technol. (Nat. Sci. Ed.)* **2013**, *36*, 75–80. (In Chinese)
14. L, J.F. Research and Design of Cylinder Used as the Primary Mirror Support of Telescope. *J. Chang. Univ. Sci. Technol. (Nat. Sci. Ed.)* **2014**, *37*, 32–37. (In Chinese)
15. Xi, X.H.; Zhang, C.J.; Hu, H.F. Layout-stiffness-correction force joint optimization of support system for ultra-large thin meniscus mirror. *Opto-Electron. Eng.* **2020**, *47*, 93–100. (In Chinese)
16. Martin, H.M.; Callahan, S.P.; Cuerden, B.; Davison, W.B.; DeRigne, S.T.; Dettmann, L.R.; Parodi, G.; Trebisky, T.J.; West, S.C.; Williams, J.T. Active supports and force optimization for the MMT primary mirror. *Proc. SPIE* **1998**, *3352*, 412–423.
17. Hovsepian, T.; Michelin, J.L.; Stanghellini, S. Design and tests of the VLT M1 mirror passive and active supporting system. In Proceedings of the Advanced Technology Optical/IR Telescopes VI, Kona, HI, USA, 25 August 1998; pp. 424–435.
18. Dierickx, P.; Enard, D.; Merkle, F.; Noethe, L.; Wilson, R.N. 8.2 metre primary mirrors of the VLT. In Proceedings of the Adaptive optics and optical structures, Hague, The Netherlands, 1 August 1990; pp. 266–274.
19. Smith, W.S. Manufacture of an 8-meter class primary mirror. *Proc. SPIE* **1994**, *1994*, 208–217.
20. Hu, H.; Luo, X.; Liu, Z.; Zhang, X.; Zhao, H. Designing a hydraulic support system for large monolithic mirror's precise in-situ testing-polishing iteration. *Opt. Express* **2019**, *27*, 3746–3760. [[CrossRef](#)] [[PubMed](#)]